LETTERS IN BIOMATHEMATICS
An International Journal

Intercollegiate Biomathematics Alliance

RESEARCH ARTICLE

OPEN ACCESS

# Characterizing Transcriptional Dynamics of HIV-1 in T-cells and Macrophages Using a Three-State LTR Model

Tin Phan[a], Catherine DeMarino[b], Fatah Kashanchi[b], Yang Kuang[a], Daniel M. Anderson[c], Maria Emelianenko[c]

[a]School of Mathematical and Statistical Sciences, Arizona State University, Tempe, AZ, USA; [b]Laboratory of Molecular Virology, School of Systems Biology, George Mason University, Manassas, VA, USA; [c]Department of Mathematical Sciences, George Mason University, Fairfax, VA, USA

**ABSTRACT**

HIV-1 affects tens of millions of people worldwide. In this work, we extend a novel three-state model of HIV-1 transcription to study the differences in the transcription process of HIV-1 in T-cells and macrophages. In particular, we find that the activation of the HIV-1 promoter in macrophages appears to take place rapidly as the Tat protein approaches a critical threshold. In contrast, the same process occurs smoother in T-cells. By examining the self-feedback loop of Tat, we observe distinct characteristic differences of the transcriptional feedback loop between macrophages and T-cells. A systematic analysis shows the stability of the positive steady state in limiting cases, with the global stability in the general case remaining an open question. Moreover, our numerical simulations and analysis demonstrate that the transcription-inhibitor's effect can be enhanced by synchronizing with standard treatments, such as combination antiretroviral therapy, to reduce the total dosages and toxicity.

**ARTICLE HISTORY**
Received December 17, 2020
Accepted July 21, 2021

**KEYWORDS**
HIV-1 transcription, F07#13, transcriptional inhibitor, treatment combination, transcriptional feedback loop, mathematical modeling

## 1 Introduction

The Human Immunodeficiency Virus Type I (HIV-1) is the causative agent of acquired immune deficiency syndrome (AIDS). Since the advent of combination antiretroviral therapy (cART) in the early 1990s, infected individuals live longer, healthier lives, and transmission rates have slowed down. However, of the 36.9 million infected worldwide, only 21.7 million people were reported to be accessing cART, and even fewer were maintaining the strict adherence required by the therapy (UNAIDSDate, 2019). Current cART regimens have been developed to target HIV-1 at almost every stage of the viral life cycle. These include fusion/entry inhibitors, which target HIV-1 cellular receptors and associated viral proteins, reverse transcriptase inhibitors, which prevent the production of viral DNA from RNA, integrase inhibitors that function to mitigate integration of the virus into host DNA, and protease inhibitors which block maturation of viral proteins. The combination of several inhibitors is effective in lowering viral titers and reducing morbidity and mortality in infected individuals (Heaton et al., 2010; Deeks et al., 2013; Mothobi and Brew, 2012). However, to date, there are no FDA-approved antiretrovirals that target HIV-1 transcription. This therapeutic gap leads to persistent, low-level viral transcription despite suppressive treatment, a concept which has been termed "leaky latency", resulting in approximately $1 \times 10^3$ copies of cell-associated viral RNA in infected cells (Furtado et al., 1999; Hatano et al., 2012; Kumar et al., 2007). While viremia is adequately controlled ($<$ 50 viral RNA/mL), cell-associated viral RNA can contribute to chronic inflammation, rapid viral rebound, immune dysfunction via direct mechanisms, stochastic production of viral proteins, or via the release of viral RNA in extracellular vesicles (McCauley et al., 2018; Akiyama et al., 2018; Ferdin et al., 2018; Narayanan et al., 2013; Sampey et al., 2016; DeMarino et al., 2018; Hladnik et al., 2017; J. Z. Li et al., 2016; Henderson et al., 2019).

Despite the presence of cART, HIV-1 can persist in viral reservoirs including long-lived memory $CD4^+$ T-cells, blood-brain barrier protected myeloid cells of the central nervous system (CNS), and low cART penetration lymphoid tissues such as lymph nodes and gut-associated lymphoid tissue (GALT) (Sengupta and Siliciano, 2018; G.-H. Li et al., 2016; Garrido and Margolis, 2015; Dave et al., 2018; Hatano et al., 2013). These reservoirs can be maintained through several mechanisms, including chro-

CONTACT Tin Phan tin.t.phan@asu.edu

matin modifications and blocks in viral transcription initiation and elongation. Although HIV-1 can persist in a latent state for long periods, activation of latently infected cells through antigen stimulation or cytokine activation can lead to the induction of HIV-1 transcription factors such as nuclear factor kappa-light-chain-enhancer of activated B cells (NF-$\kappa$B) or nuclear factor of activated T-cells (NFAT). Production of these transcription factors can, in turn, cause viral reactivation of the latent provirus leading to transcription of the HIV-1 genome and subsequent production of viral proteins (Chou et al., 2013; Mbonye and Karn, 2014; Kumar et al., 2014). Importantly, activation of the virus elicits cytolysis and immune-mediated responses to clear the virus. This mechanism has led to the development of a therapeutic strategy termed "shock and kill", an approach which takes aim at latency-mediating mechanisms, such as histone deacetylases (HDACs) (Archin et al., 2009; Lehrman et al., 2005; Wei et al., 2014), using latency-reversing agents (LRAs) to reactivate and promote immune clearance of the virus. Conversely, others have proposed an opposite strategy known as "lock and block," which focuses on promoting an inactive state of the HIV-1 LTR to inhibit viral transcription and virion production through the use of latency promoting agents (LPAs). These studies have led to the identification of several HIV-1 transcription inhibitors, which have shown success *in vitro, in vivo,* and in clinical trials (Mousseau et al., 2012, 2015; Kim et al., 2016; Jean et al., 2017; Kessing et al., 2017; Rutsaert et al., 2019; Hayashi et al., 2017)

While there is a rich literature of mathematical modeling for HIV-1 transmission at the population level (Eaton et al., 2012; Omondi et al., 2018; Velasco-Hernandez et al., 2002; Li et al., 2018) and its interaction with the immune system with or without treatments (Perelson and Nelson, 1999; Wodarz and Nowak, 2002; Wang et al., 2016; Adak and Bairagi, 2018), mathematical models at the molecular level for HIV-1 are few and far between. More recently, Chavali et al. (2015) developed and showed that a multi-state promoter HIV-1 model is perhaps better at capturing the heterogeneous reactivation of HIV-1 in response to treatments (e.g., "shock and kill" therapy) compared to the single-state promoter model. Ke et al. (2015) used a multi-state delayed activation model to study the effect of Vorinostat, a drug used in the activation of HIV-1 transcription, with experimental data. Additionally, Gupta and Dixit (2018) utilized a multi-state promoter model to study the synergy in a combination of latency-reversing therapies using stochastic simulation. Furthermore, stochastic models of HIV have also been used to provide insights into the viral rebound or eradication event of the latent reservoir (Chavali et al., 2015; Conway et al., 2019; Hill et al., 2014). Moreover, mathematical modelings have also been used to examine novel therapeutic strategies such as the effects of pulsatile verse continuous exposures to latency reversing agents (Ke et al., 2018).

In prior work, a three-state LTR model of HIV-1 transcription was developed (DeMarino et al., 2020). This model evaluates various states of the HIV-1 LTR, repressed ($\text{LTR}_R$), intermediate ($\text{LTR}_I$), and activated ($\text{LTR}_A$) in response to various stimuli, including transcription inducers. Furthermore, they modeled the transcription of two viral RNAs; a short non-coding RNA trans-activation response (TAR) element and genomic RNA (*env*), as well as levels of viral proteins Tat (trans-activator of transcription), Pr55, and p24 in response to changes in the LTR state. This model has been supported in two types of immune cells, T-cells, and myeloids, using biochemical assays that assess each parameter and model predictions at extended time frames. The model takes into account that the production of Tat, an early HIV-1 protein, only occurs during the intermediate activation state, while genomic RNA produced during the activated state is used to facilitate the production of viral particles. The simple structure of the model allows for direct incorporation of various therapies, which potentially serves as a valuable tool in evaluating viral transcription in response to various stimuli, including LRAs and LPAs.

In this work, we carry out systematic mathematical analyses of the previous model to show its biological and mathematical validity. The original model formulation utilizes a switching function to model the Tat-dependent functional responses, which limits the ability of the model to characterize differences in the transcriptional behaviors in T-cells and macrophages. Additionally, it leads to a discontinuity, which may not be biologically relevant. To address this issue, we extend the model to consider continuous Tat-dependent functional responses. To distinguish between the two model iterations, we will call the original model with the piece-wise switch **model 1** and the continuous version **model 2**. Similarly, we carry out mathematical analyses and data fitting for the new model. We provide stability results in several limiting cases; however, the global stability of the positive steady state in the general case is still an open question. By comparing the two models (switching vs. continuous response), we find observations that provide insights into the transcription process of HIV-1. Specifically, there is a clear distinction in the transcriptional behaviors between T-cells and macrophages, which is dependent on the amount of Tat protein. Finally, we use the model to study the effectiveness of an experimental transcription-inhibitor drug. Our results suggest that the Tat peptide mimetic transcriptional inhibitor (F07#13) is synchronous with standard treatment. Thus, by combining F07#13 with standard treatment such as cART, the total dosage, and the potential side effects may be reduced.

The remainder of this paper is organized as follows. In Section 2, we briefly introduce the mathematical model and describe how some treatments of HIV-1 are incorporated into the model. In Section 3, we carry out the study of the properties of the model and its extension. The main goal is to demonstrate that the model exhibits the expected biological dynamics, which entails the analyses of positive invariance, boundedness, and stability of solutions. Utilizing experimental data from DeMarino et al. (2020), we carry out parameter estimation to differentiate the dynamics between T-cells and macrophages in Section 4. An important novelty of the model is its ability to incorporate multiple treatments of HIV-1. Therefore, in Section 5, we study the effect of the transcriptional inhibitor F07#13 in combination with other drugs. Our model structure shows that Tat is involved

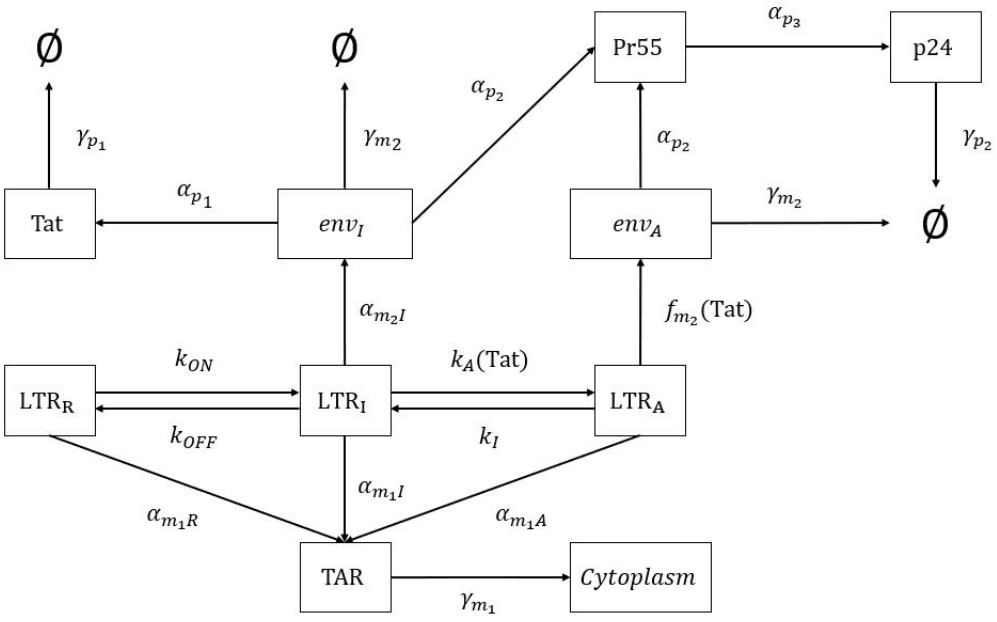


**Figure 1:** HIV-1 transcription model. Three States of LTR, e.g. repressed ($LTR_R$), intermediate ($LTR_I$), activated ($LTR_A$). The long and short RNA ($env_I$, $env_A$ and TAR), Tat, Pr 55 and p24 interactions. The figure is adapted from DeMarino et al. (2020) under a Creative Commons Attribution (CC BY) license.

in a self-feedback loop. To better understand its properties, we numerically characterize it in Section 6. Finally, we discuss our results in Section 7. Derivation of closed-form solution of model 1 and details of numerical parameter estimation are provided in the Appendix.

## 2 Mathematical Model

In DeMarino et al. (2020), the following three-state HIV-1 model (model 1) of the transcription process was derived and supported with experimental data in T-cells and macrophages.

$$\frac{d}{dt}\mathrm{LTR}_R = k_{OFF}\mathrm{LTR}_I - k_{ON}\mathrm{LTR}_R \tag{1}$$

$$\frac{d}{dt}\mathrm{LTR}_I = -\left[\frac{w_3 w_4}{w_5}k_A(\mathrm{Tat}) + k_{OFF}\right]\mathrm{LTR}_I + w_1 k_I \mathrm{LTR}_A + k_{ON}\mathrm{LTR}_R \tag{2}$$

$$\frac{d}{dt}\mathrm{LTR}_A = \frac{w_3 w_4}{w_5}k_A(\mathrm{Tat})\ \mathrm{LTR}_I - w_1 k_I \mathrm{LTR}_A \tag{3}$$

$$\frac{d}{dt}\mathrm{Tat} = \alpha_{p_1} env_I - \gamma_{p_1}\mathrm{Tat} \tag{4}$$

$$\frac{d}{dt}\mathrm{TAR} = \alpha_{m_1,R}\mathrm{LTR}_R + \alpha_{m_1,I}\mathrm{LTR}_I + \alpha_{m_1,A}\mathrm{LTR}_A - \gamma_{m_1}\mathrm{TAR} \tag{5}$$

$$\frac{d}{dt}env_I = \alpha_{m_2,I}\mathrm{LTR}_I - \gamma_{m,2}env_I \tag{6}$$

$$\frac{d}{dt}env_A = f_{m_2}(\mathrm{Tat})\mathrm{LTR}_A - \gamma_{m,2}env_A \tag{7}$$

$$\frac{d}{dt}\mathrm{Pr\,55} = \alpha_{p_2}env_I + \alpha_{p_2}env_A - (\alpha_{p_3}/w_2)P_{r55} \tag{8}$$

$$\frac{d}{dt}\mathrm{p24} = (\alpha_{p_3}/w_2)P_{r55} - \gamma_{p_2}p_{24} \tag{9}$$

The model incorporates important features of the basal and activated transcription of the HIV-1 genome. The Long Terminal Repeat (LTR) is categorized into three stages, suppressed ($LTR_R$), intermediate ($LTR_I$) and activated ($LTR_A$), similar to that

**Table 1:** Table of parameters adopted from DeMarino et al. (2020). The unit of our model parameters is [copies/ml], except for LTR, which is in percentage. We assume the experimental rates are good approximations of the true rates. DeMarino and colleagues assumed the degradation rates for Tat and p24 are taken to be $0^*$ for a short period of time, but for our analytical purpose, we will assume they are strictly positive.

| | Unit | definition | T-Cell | macrophages |
|---|---|---|---|---|
| $k_{ON}$ | [1/hr] | $\text{LTR}_R \rightarrow \text{LTR}_I$ | 5.785% | 9.245% |
| $k_{OFF}$ | [1/hr] | $\text{LTR}_I \rightarrow \text{LTR}_R$ | 1.220% | 1.228% |
| $k_A(\text{Tat})$ | [1/hr] | $\text{LTR}_I \rightarrow \text{LTR}_A$ | 3.409% | 9.010% |
| $k_I$ | [1/hr] | $\text{LTR}_A \rightarrow \text{LTR}_I$ | 0.0% | 2.451% |
| $\alpha_{m_1,R}$ | [copies/ml/hr] | $\text{LTR}_R \rightarrow \text{TAR}$ | $2.50 \times 10^4$ | $2.90 \times 10^4$ |
| $\alpha_{m_1,I}$ | [copies/ml/hr] | $\text{LTR}_I \rightarrow \text{TAR}$ | $2.80 \times 10^8$ | $7.54 \times 10^4$ |
| $\alpha_{m_1,A}$ | [copies/ml/hr] | $\text{LTR}_A \rightarrow \text{TAR}$ | $1.37 \times 10^7$ | $4.51 \times 10^5$ |
| $\alpha_{m_2,I}$ | [copies/ml/hr] | $\text{LTR}_I \rightarrow env_I$ | $3.63 \times 10^5$ | $8.13 \times 10^3$ |
| $\alpha_{m_2,A}$ | [copies/ml/hr] | $\text{LTR}_A \rightarrow env_I$ | $2.47 \times 10^6$ | $4.00 \times 10^4$ |
| $\alpha_{p_1}$ | [1/hr] | $env_I \rightarrow \text{Tat}$ | $4.00 \times 10^{-4}$ | $3.80 \times 10^{-4}$ |
| $\alpha_{p_2}$ | [1/hr] | $env \rightarrow \text{Pr}\,55$ | $1.54 \times 10^{-3}$ | $1.94 \times 10^{-3}$ |
| $\alpha_{p_3}$ | [1/hr] | $\text{Pr}\,55 \rightarrow \text{p24}$ | $1.36 \times 10^{-3}$ | $8.10 \times 10^{-4}$ |
| $\gamma_{p_1}$ | [1/hr] | Tat degradation | $0^*$ | $0^*$ |
| $\gamma_{p_2}$ | [1/hr] | $p24$ degradation | $0^*$ | $0^*$ |
| $\gamma_{m,1}$ | [1/hr] | TAR degradation | $1.17 \times 10^4$ | $2.68 \times 10^4$ |
| $\gamma_{m,2}$ | [1/hr] | $env$ degradation | $2.24 \times 10^3$ | $5.91 \times 10^2$ |
| $\text{Tat}_{crit}$ | [copies/ml] | switching limit | 3001 | 3001 |
| $v_a$ | unitless | folds of increasing | 150 | 150 |

of the model in Chavali et al. (2015). The 'OFF' states refer to the repressed and intermediate HIV-1 promoters, while the 'ON' state refers to the activated HIV-1 promoter. Here, $k_{ON}, k_{OFF}, k_A(\text{Tat})$ and $k_I$ are transition rates from one state of LTR to another as indicated in Figure 1. The total LTR is assumed to be conserved, so each LTR state in the model represents the proportion of LTR in the respective state.

Another key feature of the model is the division of viral RNA into short-non-coding RNA and long-genomic RNA, characterized by the amount of TAR and *env*, respectively. The model further divides the *env* according to its promoter LTR state, or $env_I$ and $env_A$ corresponding to $\text{LTR}_I$ and $\text{LTR}_A$, respectively. Additionally, TAR is produced by all three states of LTR, but generally at different rates. Tat is produced via the translation of a multiply-spliced mRNA, which is represented in the model as the transition from $env_I$ to Tat. The presence of Tat directly affects the activation rate of the intermediate LTR state. Hence, The coefficient $k_A(\text{Tat})$ is expected to depend on the level of Tat. Due to a quick transition to the active state, this can be approximated as a step function or a Hill function (see Section 3). The value of $\text{Tat}_{crit}$ is the estimated number of Tat required to overcome potential sequestration by TAR in the cytoplasm to allow for efficient Tat-activated transcription. Tat further enhances the transcription rate of activated LTR to produce $env_A$. This rate can also be represented by a Hill function with the same $\text{Tat}_{crit}$ value as $k_A(\text{Tat})$.

Both $env_I$ and $env_A$ are used to produce the HIV-1 gag polyprotein, Pr 55. Following its production, Pr 55 is cleaved into smaller proteins, one of which is p24, which forms the capsid and is tractable experimentally. We note that each LTR state represents the fraction of LTR in the respective state. On the other hand, the unit of all other variables is [copies/ml]. Furthermore, we take the experimentally derived rates by DeMarino et al. (2020) to be the initial approximations of the parameter values for our model. Additional details on the parameter values are listed in Table 1. One of the novel usages of this model is its ability to incorporate and study the effects of different drugs (DeMarino et al., 2020). In the model, the parameter $w_i$ (i = 1,2,3,4,5) refers to the effect of different drugs on the transcriptional dynamics of HIV-1. The current form of the model shows a possibility of incorporating multiple drugs to study their effect in combination with each other ($w_2$ - cART, $w_3$ - IR, $w_4$ PMA/PHA); however, for this work, we will focus on a particular drug F07#13. The drug F07#13, a Tat peptide mimetic, was developed to inhibit the transcription of HIV-1 virus by inhibiting Tat transactivation of the HIV-1 promoter, thereby encouraging the reverse direction from $\text{LTR}_A$ to $\text{LTR}_I$ and suppressing the activation of $\text{LTR}_I$ (Lin et al., 2017; Van Duyne et al., 2013). In the

model, these effects are represented by the parameters $w_1$ and $w_5$, respectively.

The model is used with the following initial conditions: $\mathrm{LTR}_R = 1$ (or 100%) and $\mathrm{LTR}_I = \mathrm{LTR}_A = 0$, which means that we assume that all LTRs are in the repressed state initially. In addition, $\mathrm{RNA}_1 = 0$, $\mathrm{RNA}_{2I} = 0$, $\mathrm{RNA}_{2A} = 0$, $\mathrm{Tat} = 0$, $\mathrm{Pr}\,55 = 0$ and $\mathrm{p24} = 0$ at $t = 0$.

# 3 Dynamical System Analysis

## 3.1 Global stability in case of piecewise constant switching and activation rates

In DeMarino et al. (2020), the following assumptions were made for activation rate $k_A$ and switching rate $f_{m_2}(\mathrm{Tat})$:

$$f_{m_2}(\mathrm{Tat}) = \begin{cases} \alpha_{m_2,A}/v_a & \text{if } \mathrm{Tat} < \mathrm{Tat}_{crit} \\ \alpha_{m_2,A} & \text{if } \mathrm{Tat} \geq \mathrm{Tat}_{crit} \end{cases} \tag{10}$$

$$k_A = const. \tag{11}$$

In this section we study stability of model 1, which is composed of equations (1)–(9). The assumption of LTR conservation in model 1 implies the zero steady state is always unstable given at least one of the LTRs is initially positive. Model 1 allows for the zero steady state, which is always unstable assuming at least one of the LTRs is initially positive. Additionally, all negative terms in each variable's rate equation is proportional to the variable itself. This implies that since the model starts out with at least one positive initial state (and no negative initials), no variable can become negative. Now, we shift the focus to the positive steady state of the system.

**Theorem 1.** *The system* (1)–(9) *under assumptions* (10)–(11) *has a unique positive equilibrium that is globally asymptotically stable.*

*Proof.* We prove stability in two steps. First, we decouple the system and use Bendixon-Dulac criterion to show that the isolated (decoupled) system of LTRs has a unique positive steady state that is globally asymptotically stable. It then follows directly that the entire system shares the same property.

Note that $\frac{d}{dt}[\mathrm{LTR}_R + \mathrm{LTR}_I + \mathrm{LTR}_A] = 0$, so the system of LTRs decoupled from the rest of the equations has a conservation law and the boundedness of $\mathrm{LTR}_R, \mathrm{LTR}_I, \mathrm{LTR}_A$ follows immediately. We consider the reduced two-dimensional system:

$$\frac{d}{dt}[\mathrm{LTR}_I] = k_{ON} - (k_A + k_{OFF} + k_{ON})\mathrm{LTR}_I + (k_I - k_{ON})\mathrm{LTR}_A \tag{12}$$

$$\frac{d}{dt}[\mathrm{LTR}_A] = k_A\mathrm{LTR}_I - k_I\mathrm{LTR}_A. \tag{13}$$

The nullclines of $\mathrm{LTR}_I$ and $\mathrm{LTR}_A$ are lines that intersect in the first quadrant, thus the system has a unique positive fixed point. Let $f(\cdot) = \frac{d}{dt}[\mathrm{LTR}_I]$ and $g(\cdot) = \frac{d}{dt}[\mathrm{LTR}_A]$. Observe that

$$\frac{\partial f}{\partial(\mathrm{LTR}_I)} + \frac{\partial g}{\partial(\mathrm{LTR}_A)} = -(k_A + k_{OFF} + k_{ON}) - k_I < 0. \tag{14}$$

By Bendixson-Dulac criterion, the system does not have a periodic orbit. Therefore the unique positive steady state is globally asymptotically stable, by Poincaré - Bendixson theorem. Stability of the original system follows by simply substituting equilibrium values of LTRs into the rest of the equations. For instance, consider the rate equation for TAR. Let $N_{\mathrm{LTR}}$ denote $\alpha_{m_1,R}\mathrm{LTR}_R^* + \alpha_{m_1,I}\mathrm{LTR}_I^* + \alpha_{m_1,A}\mathrm{LTR}_A^*$. Then in the limit as $t \to \infty$, the rate of change of TAR becomes:

$$\frac{d}{dt}(\mathrm{TAR}) = N_{\mathrm{LTR}} - \gamma_{m_1}\mathrm{TAR} \tag{15}$$

This implies the unique positive steady state $\mathrm{TAR}^* = N_{\mathrm{LTR}}/\gamma_{m_1}$ is globally stable. Similar argument holds for the remaining variables. Note that the steady state of $env_A$ takes the form of a step function

$$env_A^* = \begin{cases} \frac{\alpha_{m_2,A}\mathrm{LTR}_A^*}{v_a\gamma_{m_2}} & \text{if } \mathrm{Tat}^* < \mathrm{Tat}_{crit}, \\ \frac{\alpha_{m_2,A}\mathrm{LTR}_A^*}{\gamma_{m_2}} & \text{if } \mathrm{Tat}^* \geq \mathrm{Tat}_{crit}, \end{cases} \tag{16}$$

where $\mathrm{Tat}^* = (\alpha_{p_1} env_I^*)/\gamma_{p_1}$. □

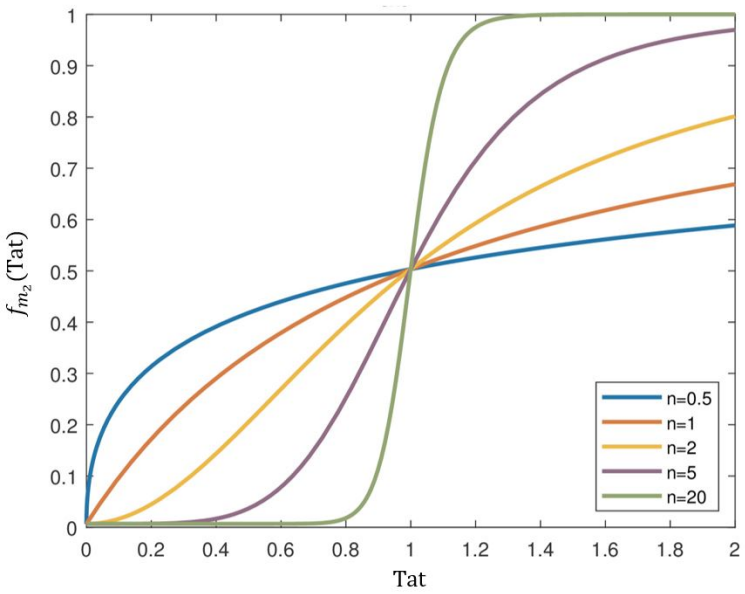


**Figure 2:** The shapes for the Hill function in Equation (17) for different values of $n$. The smooth curves of $f_{m_2}(\text{Tat})$ quickly converge to a switch function between 0 and 1 (at $\text{Tat}_{crit} = 1$) for increasing value of $n$. A similar observation is seen for the Hill function in Equation (18).

The existence of the globally asymptotically stable positive steady state of the system implies that the amount of virus would increase to a stable level once the activation of HIV-1 takes place. For model 1, it is straightforward to describe the steady-state's dependence on each of the parameters by obtaining the corresponding eigenvalues of the Jacobian matrix. This can provide useful information on the rate of growth/decay of each variable to further analyze the system and its potential modifications. On the other hand, a detailed examination of the sensitivity to each of the parameters is outside of this work scope.

## 3.2 Stability in case of switching and activation rates continuously depending on Tat

The model described above contains discontinuities due to the switching of the $f_{m_2}$ regimes based on Tat level, which may not be biologically valid. Furthermore, the switching function limits the model's ability to distinguish the transcriptional dynamics as Tat approaches the critical threshold $\text{Tat}_{crit}$ for T-cells and macrophages. In what follows, we introduce a continuous version of the existing model by modifying the switches to the following form of Hill function:

$$f_{m_2}(\text{Tat}) = \frac{\alpha_{m_2,A}}{v_a} \frac{1 + v_a(\text{Tat}/\text{Tat}_{crit})^n}{1 + (\text{Tat}/\text{Tat}_{crit})^n}, \quad v_a > 1 \tag{17}$$

$$k_A(\text{Tat}) = \frac{\beta_{m_2,A}}{v_b} \frac{1 + v_b(\text{Tat}/\text{Tat}_{crit})^m}{1 + (\text{Tat}/\text{Tat}_{crit})^m}, \quad v_b > 1 \tag{18}$$

Figure 2 shows that $f_{m_2}$ converges to the Heaviside step function as $n$ increases, asymptotycally approaching the form considered in the previous section, to characterize the Tat-dependent rates in the transcription process. Not to impose additional assumptions, we reserve two different Hill constants $n$ and $m$ for $f_{m_2}(\text{Tat})$ and $k_A(\text{Tat})$. While $n$ often takes value between 2 and 3 in literature, or 1 in Chavali et al. (2015), the possible biologically relevant ranges of $n$ and $m$ are all real numbers greater than or equal to 1. For $n < 1$, the activation starts rapidly at $\text{Tat} = 0$, which is not what we would expect biologically, so we would only consider $n \geq 1$. In this case, model 2 is the system (1)–(9) with the modification in equations (17) and (18). This modification does not change the fact that all negative terms in the rate of change of a variable are still associated with the corresponding variable, so similar to model 1, model 2 is also positively invariant.

The introduction of the continuous functional responses allows for a more interesting coupling of the dynamics between different variables; however, the system's overall dynamics still do not rely on TAR, Pr55, and p24. Additionally, within the remaining six equations, $env_A$ does not contribute to the dynamics of the other five, and LTR is conserved. Thus, we start our analysis on the reduced system of four differential equations (2), (3), (4), (6).

Define $x = \text{LTR}_I$, $y = \text{LTR}_A$, $s = env_I$, $v = \text{Tat}$, $a_1 = k_{ON}$, $a_2 = k_I - k_{ON}$, $a_3 = k_{ON} + k_{OFF}$, $a_4 = k_I$, $a_5 = \alpha_{p_1}$, $a_6 = \gamma_{p_1}$, $a_7 = \alpha_{m_2,I}$, $a_8 = \gamma_{m_2}$, $a_9 = \beta_{m_2,A}/v_b$, $a_{10} = v_b/(\text{Tat}_{crit})^n$ and $a_{11} = 1/(\text{Tat}_{crit})^n$. Note that $a_{10} = v_b a_{11}$, so since we take $v_b$ to be

strictly larger than 1, $a_{10} > a_{11}$. With these notations, the system takes on the form:

$$x' = a_1 + (a_4 - a_1)y - \left(a_3 + a_9\frac{1 + a_{10}v^m}{1 + a_{11}v^m}\right)x \tag{19}$$

$$y' = a_9\frac{1 + a_{10}v^m}{1 + a_{11}v^m}x - a_4y \tag{20}$$

$$s' = a_7x - a_8s \tag{21}$$

$$v' = a_5s - a_6v. \tag{22}$$

Similar to model 1, model 2 contains a zero steady-state that is always unstable, given at least one of the initial conditions for LTR stages is positive. Thus, we focus our analysis on the positive steady state. Note that for $m < 1$, the Hill function exhibits dynamics that are unexpected for our biological system, see Figure 2, so we discard that case. For $m \geq 1$, we show that the system contains a unique positive steady state (see Proposition 1 in the Supplementary Materials). The positivity of the unique nontrivial steady state of our system helps establish its biological validity. However, it does not rule out the possibility of finding a steady-state arbitrarily close to 0, which is unrealistic when HIV-1 viral load stays low but away from 0. For this reason, we establish a proposition that establishes lower bounds (and upper bounds) on all system variables.

Recall that the system described in Equations (19)–(22) is permanent if there are positive constant M and N such that

$$\limsup_{t\to\infty} \max\{x(t), y(t), s(t), v(t)\} < M,$$

and

$$\liminf_{t\to\infty} \min\{x(t), y(t), s(t), v(t)\} > N.$$

We will show that the system in Equations (19)–(22) is permanent in the above sense for $m \geq 1$. By construction, $x$ and $y$ are bounded above by 1, so we only need to show they also have a positive lower bound. This results in the following proposition (proof in Section A.2 of the Supplementary Materials).

**Proposition 1.** *Define* $m_x = \frac{\min\{a_1, a_4\}}{a_3 + a_9 v_b}$ *and* $m_y = \frac{a_9}{a_4}m_x$, *then* $0 < m_x \leq \liminf_{t\to\infty} x$ *and* $0 < m_y \leq \liminf_{t\to\infty} y$.

From Proposition 1, it is straightforward to show that $s$ and $v$ also have positive lower and upper bounds. Thus we state the following Lemma, which also guarantees that model 2 with $k_A(\text{Tat})$ and $f_{m_2}(\text{Tat})$ continuously dependent on Tat is also permanent.

**Lemma 1.** *The system in Equations (19)–(22) is permanent.*

## 3.3 Two alternative 3-dimensional approximations

Even with the previous reduction, the asymptotic dynamics of the reduced system (19)–(22) is still difficult to study. Thus, we examine two alternative models that capture the asymptotic behavior of the reduced system. Consider the following **QSS system:**

$$x' = a_1 + (a_4 - a_1)y - \left(a_3 + a_9\frac{1 + a_{10}v^m}{1 + a_{11}v^m}\right)x \tag{23}$$

$$y' = a_9\frac{1 + a_{10}v^m}{1 + a_{11}v^m}x - a_4y \tag{24}$$

$$v' = a_5\frac{a_7}{a_8}x - a_6v. \tag{25}$$

Alternatively, one can treat the $s$ compartment as a delay factor in the link between $x$ and $v$. In other words, we assume $s(t) \approx \frac{a_7}{a_8}x(t - \tau)$, where $\tau$ is a pre-determined time delay ($\tau \approx 1/a_8$). This leads to the following **Delay system:**

$$x' = a_1 + (a_4 - a_1)y - \left(a_3 + a_9\frac{1 + a_{10}v^m}{1 + a_{11}v^m}\right)x \tag{26}$$

$$y' = a_9\frac{1 + a_{10}v^m}{1 + a_{11}v^m}x - a_4y \tag{27}$$

$$v' = a_5\frac{a_7}{a_8}x(t - \tau) - a_6v. \tag{28}$$

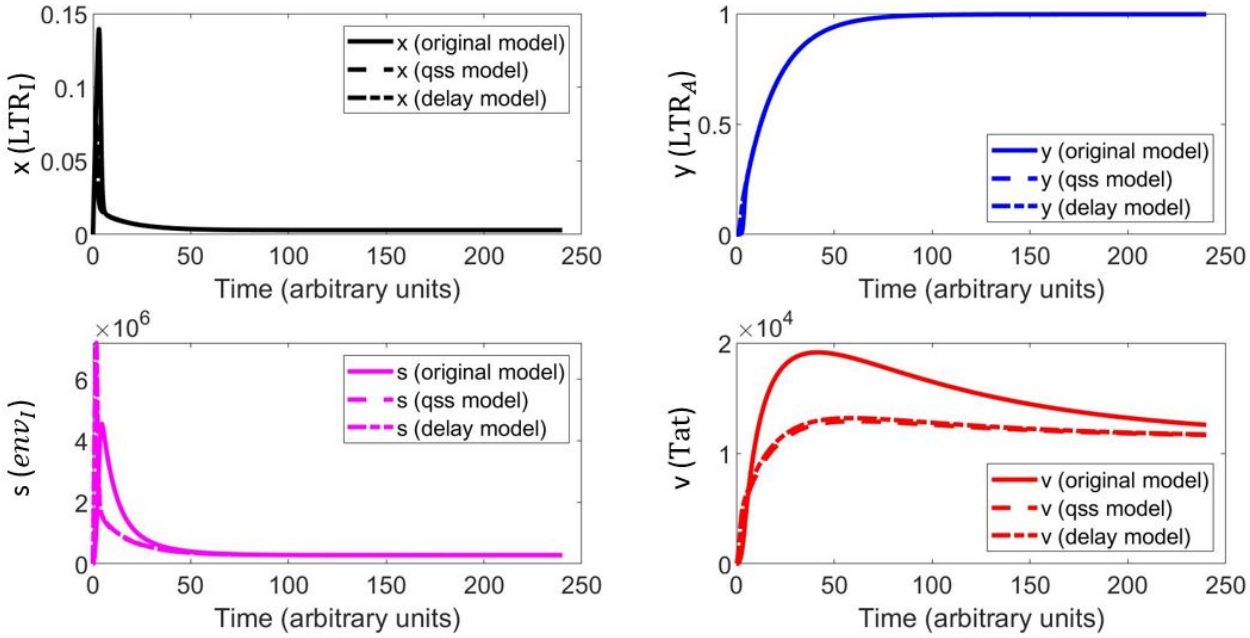


**Figure 3:** Numerical comparison of the 4-dimensional model (19)–(22), QSS model (23)–(25) and Delay model (26)–(28). The y-axis shows the new variables and what it stands for in the original model. Parameter values are for T-cells. While all models show similar behavior for $x$ and $y$ dynamics, reduced models underestimate the growth of $v$ variable and there are differences in transient behavior for the $s$ variable. Nonetheless, asymptotic behaviors of all models are similar.

In Figure 3, we provide a computational comparison of these two models against the original one. Both approximations are able to capture the asymptotic behavior of the system, but there are noticeable differences in transient dynamics, as expected. Since the Delay model does not offer significant advantages over the QSS model in capturing long-term system behavior based on this calculation, we will focus on the QSS model in our stability analysis. We note that the Delayed model might be useful if a more careful analysis of the transient mode is of interest.

### 3.4 Stability of the QSS model

For the quasi-steady state model (23)–(25), its boundedness, positive invariance and the existence of a unique positive steady state are direct consequences of the results we established earlier for the original 4-dimensional model. Thus, we only need show local asymptotic stability for the positive steady state. We apply the Routh-Hurwitz criterion to arrive at the following proposition (proof in Section A.3 of the Supplementary Materials).

**Proposition 2.** *The positive steady state of the QSS system is locally asymptotically stable.*

The complete global stability result is difficult to obtain even for the quasi-steady state system (using standard Lyapunov functions) and may not yield additional insights. Instead, we observe that $\text{Tat}_{crit}$ is several orders of magnitude smaller than the value of Tat shortly after the experiment starts. This means model 2 is quickly reduced to model 1 unless $\text{Tat}_{crit}$ is significantly larger. Qualitatively, this means that if the production rate of Tat is high enough, then we can expect the new model to show similar dynamical behavior to the original system (e.g., the positive steady state is globally asymptotically stable). A similar observation should hold for a very low production rate of Tat.

In Figure 4 we numerically study the dependence of steady-state on varying parameters over a reasonable range. The following results are representative of the study. They show that under reasonable parameter ranges, the positive steady state is always stable. These observations suggest that the unique fixed point is expected to be global stable for model 2.

## 4 Qualitative Comparison of Model 1 and Model 2

DeMarino et al. (2020) collected time series data for TAR and total *env* RNA. Previously, standard least squares method was used to fit model 1 given by (1)–(9) under assumptions (10)–(11) to all the data points simultaneously. We utilize the same method for

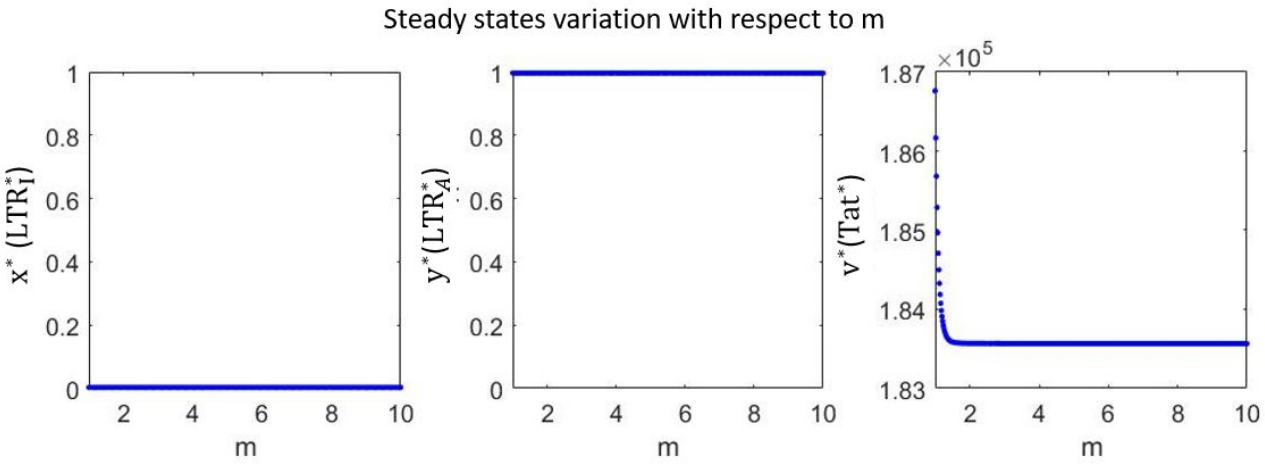


**Figure 4:** Effects of varying parameter $m$ on the asymptotic behaviors of the QSS system (23)-(25). Note that the positive steady state for $x$ is very small but positive. The figure is representative of simulation results for all other parameters of the model. We observe no changes to the stability of positive steady state of the system with respect to biologically realistic variations of all parameters.

direct comparison with the behavior of model 2 specified by (1)–(9) under assumptions (17)–(18). We use the estimated values of the parameters presented in Table 1 as our base line for the fitting procedure. Our main goal is to evaluate the capability of model 2 to fit the data in comparison to model 1.

The function `fmincon` in MATLAB, which uses the *interior point algorithm*, is used to estimate these parameters. Additionally, the range for $v_b$ is taken to be $[1, 200]$ (i.e. around the value of $v_a$) and the ranges for $n$ and $m$ are taken to be $[1, \infty)$ since there are no known biological constraints for their upper bound. Further details of the fitting procedure and estimated values are presented in Section A.4 of the Supplementary Materials.

Figures 5 and 6 show that both models produce similar fits for T-cells; however, model 2 gives superior fit to the macrophages data. Specifically, model 2 can capture the downward trend near the end of the experiment. In Figure 7, we note that the effect of Tat on the dynamics of the system quickly saturates similarly in both models. However, compared to model 1, model 2 predicts a lower level of Tat in both cases, especially in T-cells. Based on model 2, Tat's level is similar in both T-cells and macrophages, whereas model 1 predicts a higher level of Tat.

## 5 Combining F07#13 with Standard Treatments for HIV-1

Concerning the drug F07#13, when administered, the values of $w_1, w_5$ increase higher than 1. This leads to an increase in the steady states $\text{LTR}_I^*$ and $\text{LTR}_R^*$, while $\text{LTR}_A^*$ will decrease. Consequently, the value of $env_I^*$ will increase, while $env_A^*$ will decrease. These effects eventually affect the production of Pr 55. Since Pr 55 can be used as a tracker for viral protein production, the effect of F07#13 may potentially be studied by looking at how it affects the dynamics of Pr 55. Recall that model 1 is globally asymptotically stable; thus, we can use the steady states to analyze drug effectiveness.

First, we demonstrate that it is not trivial that treatment using F07#13 will reduce the production of Pr 55. Note that F07#13 reduces the activation rate of LTR, so it negatively affects the proportion of $\text{LTR}_A$ and consequentially the production of $env_A$ and the corresponding production of Pr 55 from $env_A$. However, this comes at the cost of increasing the proportion of $\text{LTR}_I$, which increases the production of $env_I$ that also contributes to the production of Pr 55 at an equal rate to that of $env_A$. The contributions of $env_I$ and $env_A$ are reflected in the final state $\text{Pr}\,55^*$ at an equal rate of $\frac{\alpha_{p_2} w_2}{\alpha_{p_3}}$. In other words, it is not obvious whether or not F07#13 effectively decreases Pr 55. For instance, consider their ratio when $w_2 = w_3 = w_4 = 1$ (only F07#13 is present) and $\text{Tat}^* \geq \text{Tat}_{crit}$:

$$\frac{env_I^*}{env_A^*} = w_1 w_5 \frac{\alpha_{m_2,I}}{\alpha_{m_2,A}} \frac{k_I}{k_A}.$$

This shows that F07#13 affects the relative concentration of $env_I^*$ and $env_A^*$; however, the actual amount of increasing/decreasing due to F07#13 is not clear. For the above reasons, we take a different approach to derive the following condition for F07#13 to

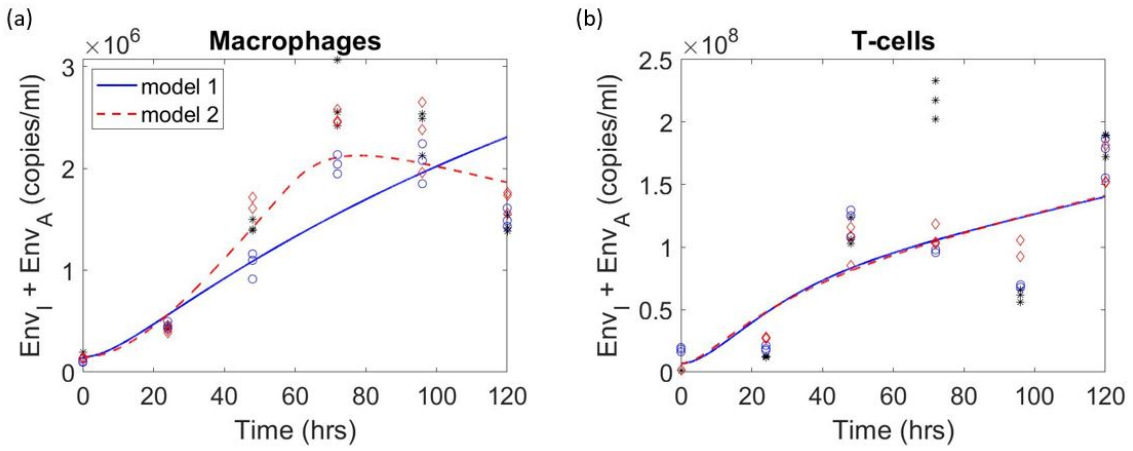


**Figure 5:** Comparison of model 1 and model 2 fitted to *env* data in both T-cells and macrophages. (a) *env* data and the fitted models' behavior in macrophages. (b) *env* data and the fitted models' behavior in T-cells.

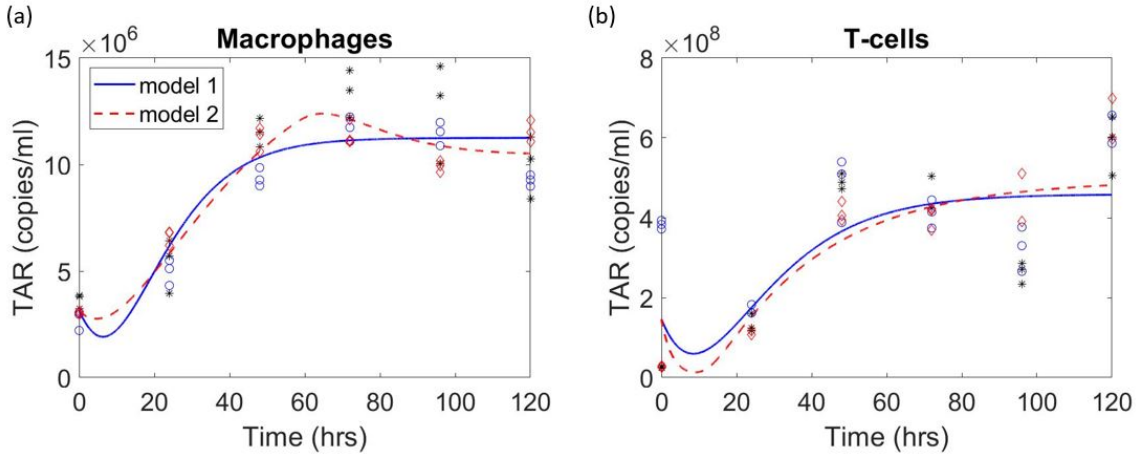


**Figure 6:** Comparison of model 1 and model 2 fitted to TAR data in both T-cells and macrophages. (a) TAR data and the fitted models' behavior in macrophages. (b) TAR data and the fitted models' behavior in T-cells.

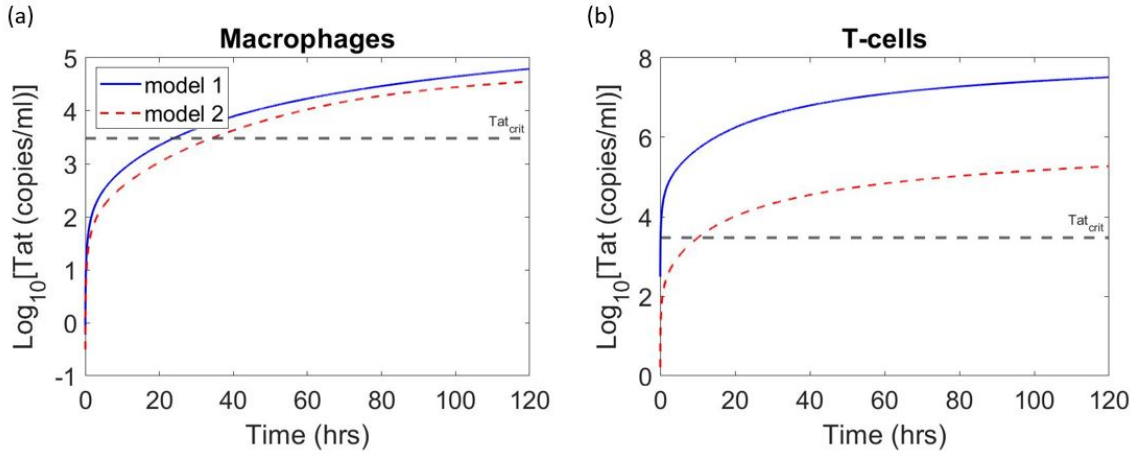


**Figure 7:** The comparison of Tat (log scale for the y-axis) resulted from the fitting of model 1 and model 2 to TAR data and *env* data in both T-cells and macrophages. The dashed horizontal line denotes the Tat-critical threshold. (a) Tat dynamics in macrophages. (b) Tat dynamics in T-cells.

be effective in reducing the amount of Pr 55 (for details see subsection A.5 of the Supplementary Materials).

$$\frac{\alpha_{m_2,I}}{\alpha_{m_2,A}} < 1 + \frac{k_{OFF}}{k_{ON}}. \tag{29}$$

Alternatively, it can be rearranged as

$$\frac{\alpha_{m_2,A}}{\alpha_{m_2,I}} > \frac{k_{ON}}{k_{ON} + k_{OFF}}. \tag{30}$$

This suggests that for the drug F07#13 to be effective in reducing the equilibrium value of Pr 55, the ratio between the rates of production $\alpha_{m_2,A}$ and $\alpha_{m_2,I}$ must be greater than the contribution of $k_{ON}$ in the sum $k_{ON} + k_{OFF}$. It is surprising that the effectiveness of F07#13 does not depend on the transition rates between $\text{LTR}_I$ and $\text{LTR}_A$. We remark that this condition is necessary because even though F07#13 may appear to be effective initially, it may not decrease the equilibrium value of Pr 55, see Figure 9.e in DeMarino et al. (2020). Furthermore, this result is only valid close to $w = 1$, where $w = \frac{1}{w_1 w_5}$ (or for small dose), so it may not be applicable in general. However, the idea is the same in the general case, so for the drug to be effective eventually, we require $\frac{d}{dw}\,\text{Pr}\,55^*(w) > 0$ for $0 < w \leq 1$, or equivalently,

$$\left[1 - \frac{k_{ON}k_A}{k_I(k_{ON} + k_{OFF}) + k_{ON}k_A w}\left(w + \frac{\alpha_{m_2,I}}{\alpha_{m_2,A}}\frac{k_I}{k_A}\right)\right] > 0. \tag{31}$$

If this inequality holds, then we can expect the F07#13 to be effective in decreasing Pr 55, which will subsequently decrease the production of p24. Similar analysis holds when $\text{Tat}^* < \text{Tat}_{crit}$. Additionally, if all drugs are considered, e.g. $w_2, w_3, w_4 > 1$, then the condition becomes:

$$\left[1 - \frac{k_{ON}k_A w^*}{k_I(k_{ON} + k_{OFF}) + k_{ON}k_A w^* w}\left(\frac{w}{w^*} + \frac{\alpha_{m_2,I}}{\alpha_{m_2,A}}\frac{k_I}{k_A}\right)\right] > 0 \tag{32}$$

where $w^* := w_3 w_4$. This suggests the effect of the F07#13 drug can be enhanced by the other drugs. Equation (32) represents the generalization of (29), accounting for other drugs and including all values of $w \in (0,1)$. Figure 8 demonstrates an example of the condition (29).

The maturation of Pr 55 to p24 is targeted by the standard HIV-1 treatment cART (recall that this is represented by the parameter $w_2$ in the model). In Figure 9, we show the possible effects of combining F07#13 and cART. Figure 9(a) shows that while both cART and F07#13 are effective in reducing the number of p24 at 200 hours, when used in combination, the level of p24 is reduced further. Additionally, we provide a sample synergy map between F07#13 and cART (without accounting for toxicity) in Figure 9(b). In that figure, an arbitrary p24 level (e.g., $1.2\times10^6$) is used to emphasize the synergistic effect between the two treatments. The light grey area represents p24 level above the threshold, while the dark grey area represents p24 level below the threshold. Since the boundary leans toward a higher dosage of F07#13, this shows that there is some synergetic interaction between the two drugs.

However, because we do not consider the toxicity level and there is some lack of confidence in the exact values of the drug effect/amount, further study with more comprehensive data is required to validate our results and estimate the specific value of the synergy between F07#13 and cART. Finally, we remark that while we do not have the global asymptotic stability for model 2, our previous mathematical and computational analyses suggest that it is also globally asymptotically stable. Since both models' asymptotic behaviors are similar (if converged), we expect the drug effectiveness study in this section to hold similarly for model 2.

## 6 Feedback Loop Characterization

The previous section implies the existence of non-trivial behaviors involving Tat in a feedback loop. Hence, we examine this feedback loop further in this section by characterizing whether it is a self-activating or self-inhibiting loop. For the characterization of the feedback loop involving Tat, we define

$$\alpha := \frac{\partial}{\partial \text{Tat}}\frac{d\text{Tat}}{dt} \tag{33}$$

$$= \alpha_{p_1}\frac{\alpha_{m_2,I}\text{LTR}_I - \gamma_{m_2} env_I}{\alpha_{p_1} env_I - \gamma_{p_1}\text{Tat}} - \gamma_{p_1}. \tag{34}$$

Tat is involved in a self-activating feedback loop if $\alpha > 0$. On the other hand, if $\alpha < 0$, then Tat is involved in a self-inhibiting feedback loop.

In Figure 10, we attempt to numerically characterize the feedback loop involving Tat using model 2. Both characterizations of the self-feedback loop of Tat share a similar shape but describe two different phenomena. In macrophages, the feedback loop

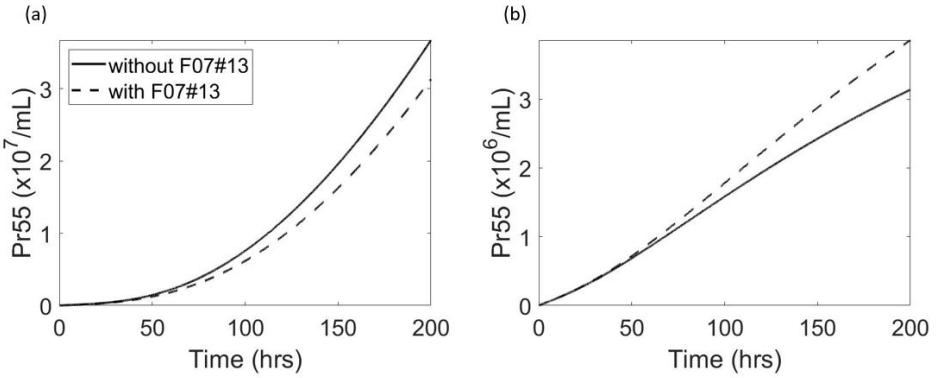


**Figure 8:** Using the parameters for model 1 for T-cells given in Table 1, we compare the effect of F07#13 on the dynamics of Pr 55 for different levels of $\alpha_{p_1}$. (a) Without modification to the parameter, the condition (29) is satisfied and F07#13 is effective in reducing the level of Pr 55. (b) By reducing the parameter $\alpha_{p_1}$ 1000 folds, we break the condition (29), leading to the ineffectiveness of F07#13 in reducing the level of Pr 55.

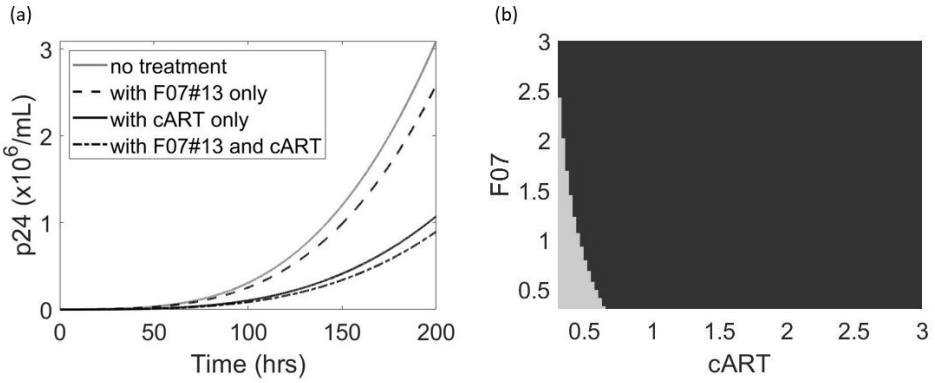


**Figure 9:** Using the parameters for model 1 for T-cells given in Table 1, we compare the effect of F07#13 and cART on the dynamics of $p24$. The effect of cART is set at 3 ($w_3 = 3$), meaning it reduces the production of $p24$ from Pr 55 to a third. (a) The combination of F07#13 and cART reduces the level of $p24$ lower than either treatment alone. (b) Level of $p24$ at 200 hours with varying amounts of F07#13 and cART. Both axes represent the fold change in the drug level of F07#13 and cART. We use an arbitrary threshold of $1.2 \times 10^6$ to emphasize the effect in varying F07#13 and cART with respect to one another. The light grey area represents $p24$ level above the threshold, while the dark grey area represents $p24$ level below the threshold.

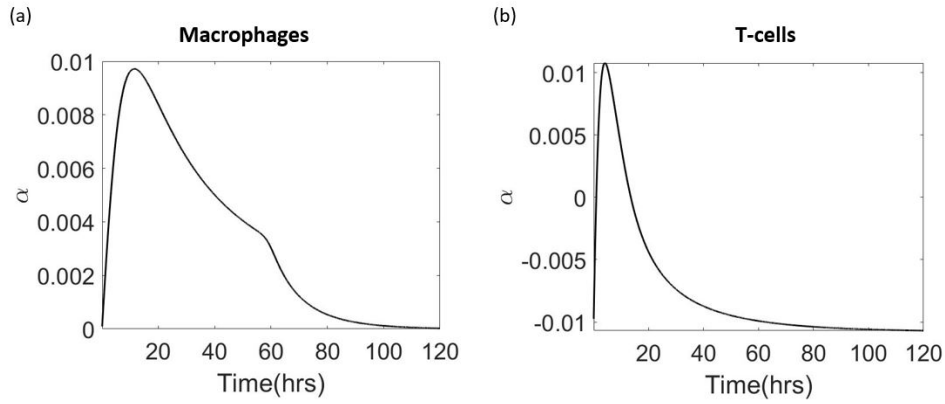


**Figure 10:** Characterization of the feedback loop involving Tat using model 2 with parameters presented in Table 1 in the Supplementary Materials. (a) In macrophages, Tat is in a self-activating feedback loop from 0 to 120. (b) In T-cells, the self-feedback loop of Tat is initially self-inhibiting but quickly becomes self-activating and remains so briefly before regressing to a self-inhibiting feedback loop.

**Table 2:** Characterization of Tat feedback loop in HIV-1 as observed from Figure 10.

| Duration | Initial time | Near the critical threshold | Final time |
|---|---|---|---|
| Macrophages | neutral → self-activating | (decreasing strength) self-activating | self-activating → neutral |
| T-cells | self-inhibiting → self-activating | self-activating → self-inhibiting | self-inhibiting |

is entirely self-activating for the 120-hour duration of the simulation. The strength of the self-feedback loop rapidly increases initially, then after reaching a peak around the 20-hour mark, its strength drops in a biphasic fashion toward 0. On the other hand, the Tat self-feedback loop in T-cells starts as a self-inhibiting loop, then rapidly becomes a self-activating loop briefly before returning to a self-inhibiting loop. The observations in Figure 10 are summarized in Table 2.

# 7 Discussion

HIV-1 continues to be a serious problem worldwide. Despite tremendous efforts, the ultimate cure for HIV-1 is yet to be discovered. Standard treatments, such as cART, target multiple key points in the production of HIV; however, a low level of viral products persists during latency partially due to the lack of an FDA-approved drug to inhibit the viral transcription process. This chronic state of HIV-1 is often accompanied by neurocognitive disorders in many patients using cART (Heaton et al., 2010; Mothobi and Brew, 2012). Additionally, experimental drugs often fail during the phase of clinical trials (Khanna, 2012; Hwang et al., 2016). This is partially due to a lack of quantitative methods to predict the drug's efficacy and toxicity, especially in combination with other drugs. Thus, a basic understanding of these mechanisms for HIV-1 is crucial for the successful development of new therapies.

In this work, we carry out systematic analyses of the properties of a model of the HIV-1 transcription process that incorporates three distinct promoter states (repressed, intermediate, and activated), introduced in DeMarino et al. (2020). We propose a smooth version of the model to address the discontinuity in the original model formulation's functional response. Comparing the two versions of the model reveals interesting biological insights into the transcription process for HIV-1. We also carry out a theoretical study of the effectiveness of the experimentally-driven drug F07#13 and characterization of the dynamics of Tat. We summarize and further discuss our findings below.

**The basic biological properties and stability results of both models.** We show that both models are positively invariant, given at least one of the LTR states is initially positive. Additionally, all solutions in model 1 tend to a positive steady state. The steady state's closed-form allows for direct quantification of the expected viral level and its exponential transcriptional rates, allowing us to assess their effect on the transcription process. Model 2 shares many similarities with model 1. We also show that its solutions are permanent, and the system also exhibits a unique positive steady state. However, the complete stability analysis is difficult due to the nonlinear functional form of Tat-dependent activation. Thus, we approximate the asymptotic behavior of model 2 using a QSS model, which allows us to show that the unique positive steady state is locally asymptotically stable. Furthermore, we remark that the dynamics of model 2 approaches that of model 1 in the limit when the production of Tat is either very high or very low. Thus, we conjecture that the positive steady state is globally stable in the general case.

**Qualitative comparison between T-cells and macrophages.** To test the capability to capture the transcriptional dynamics of HIV-1, we carry out a standard data fitting procedure using both models. Figures 5 and 6 show that overall model 2 is better at describing the qualitative trend in the data. Now, recall that the larger the values of $n$ and $m$ are, the more alike to a switching function $k_a(\text{Tat})$ and $f_{m_2}(\text{Tat})$ become, see Figure 2. Additionally, $v_a$ and $v_b$ represent the folds of increase in the rate of activation and $env_A$ production, respectively. We note a significant difference between these values in macrophages and T-cells for model 2. In macrophages, the values of $n, m, v_a, v_b$ are about one order of magnitude larger than their respective in T-cells (see Table 1 in the Supplementary Materials). This suggests more abrupt changes in the level of transcriptional dynamics as Tat approaches the critical threshold $\text{Tat}_{crit}$ in macrophages than T-cells. Meaning, it may be more difficult to detect and monitor the activation of HIV-1 in macrophages until the amount of Tat has passed the critical threshold. Furthermore, since the rates of transcriptional activation are different between T-cells and macrophages, drugs that target each specific cell type can be used together in a way that minimizes the overall toxicity and maximizes effectiveness.

Understanding the dynamics of Tat is crucial to a complete picture of the transcriptional dynamics of HIV-1, especially with the regards to the contribution of Tat to the latency reversing event (Weinberger et al., 2005; Weinberger and Shenk, 2006). Thus, we attempt to define and numerically characterize the self-loop of Tat (see Figure 10). Tat is part of a transcriptional feedback loop which is often considered to be a strongly positive transcriptional feedback loop that also involved the positive

transcription elongation factor b (P-TEFb) (Weinberger et al., 2005; Kim and Sharp, 2001; Karn, 2000), but the specific circumstances and the properties of the feedback loop are not well-understood. Thus, we numerically examine the characteristics of the self-loop of Tat, which directly impacts the properties of the overall loop. In macrophages, Tat is involved in a self-activating loop for the entirety of the 120-hour experiment, while Tat switches between a self-inhibiting to a self-activating and back to a self-inhibiting loop in T-cells. This qualitative characterization of the self-loop of Tat is consistent in both models. The surge observed in Figure 10 is perhaps due to the drugs used to induce the transcription activation. However, the end behaviors (around the 0- and 120-hour marks) suggest that without transcription inducers or once a sufficient amount of Tat is produced to reach efficient viral replication, the self-feedback loop of Tat becomes neutral in macrophages or self-inhibiting in T-cells, see Table 2. This finding is biologically sensible because we would expect a decrease in the production of Tat once efficient viral production is reached, otherwise, additional production of Tat would result in more burden in the viral production with diminishing return.

Biologically, the Hill coefficients $m$ and $n$ with a value greater than 1 represent Tat cooperativity in the activation of HIV-1. While there is a lack of evidence to support Tat cooperativity in literature, the assumptions of our model formulation and numerical simulations suggest that this is the case. Recall that in our model, Tat is needed to overcome the potential sequestration by TAR for faster transcription. For this reason, our model incorporates Tat in a self-feedback loop. Indeed, our characterization suggests that in both macrophages and T-cells, this self-feedback behavior can quickly become positive (at least initially) or self-activating, see Figure 10. Thus, it means that initially, the more Tat there is, the faster Tat accumulates, leading to a more disruptive change (e.g., switch function). As a consequence, the Hill coefficients are estimated to be greater than 1 (e.g., recall that the Hill function only produces this phenomenon for $n > 1$, see Figure 2). The idea that cooperativity can arise from positive feedback loop can also be found in other study (Andreu-Moreno et al., 2020). Additionally, it is worth pointing out that the cumulative value of $\alpha$ over 120 hours is more prominent in macrophages than in T-cells, which corresponds to the larger values of $m$ and $n$ in macrophages compared to T-cells.

**The effectiveness of the transcriptional inhibitor F07#13 and its interaction with standard treatments.** Previous simulations in Figure 9(e) in DeMarino et al. (2020) shows that while a drug (e.g., F07#13) may appear to be ineffective (or effective) initially, the result may differ. This leads to our study of the potential effect of the HIV-1 transcription inhibitor drug F07#13 based on the steady-state's closed-form expression for model 1. We establish a condition that ensures the overall effectiveness of F07#13 – that can be carried out similarly for other drugs. Furthermore, we generalize this condition to include the effect of other drugs, which allows a study of combination therapy to be carried out naturally.

Our simulation and analyses suggest that the incorporation of HIV-1 transcription inhibitors, such as F07#13, in combination with other HIV-1 treatments may improve their efficacy due to their potential synergy with one another, see Figure 9. Furthermore, we observe that the condition in equation 30 implies that the effectiveness of F07#13 only depends on the transition rates between $\text{LTR}_R$ and $\text{LTR}_I$ (and not the activation rate from $\text{LTR}_I$ to $\text{LTR}_A$). This means a drug that suppresses the transition from $\text{LTR}_R$ to $\text{LTR}_I$ (or enhances the reverse transition) would work well with F07#13.

**Limitation and future work.** Using a combination of mathematical analysis and computational simulations, we show interesting observations in the transcriptional dynamics of HIV-1, especially the differentiation in behaviors in T-cells and macrophages. While our model is constructed based on current biological knowledge and supported with experimental data, it has some strong assumptions and limitations. The model is constructed for the analysis of short term transcriptional dynamics of HIV-1. Thus, many of the rate parameters are linear, making it unsuitable for studying the long term dynamics of HIV-1. Furthermore, certain parameters are difficult to observe or estimate from experimental data alone, which necessitates our data fitting process. Additionally, the model does not account for the difference between degradation and exit rates of certain variables. While the model can be modified to account for the extracellular contents to distinguish between degradation and exit rates, this would further increase the model's complexity.

Regarding numerical aspects, we carry out basic data fitting and simulations to show the capability of the model to capture the transcriptional dynamics in the data and demonstrate the theoretical results. Extensive sensitivity analysis and perhaps more sophisticated data fitting schemes should be carried out in the future for better uncertainty quantification of the estimated parameter values and model findings. Finally, while we consider the primary effect of the transcriptional inhibitor F07#13 to reduce the activation rate of LTR, other secondary effects of F07#13 are not taken into account. Thus, a direct extension would be to account for all known effects of F07#13 and cART (along with their potential toxicity) in the study of treatment combination. Such a study may prove useful in drug development for clinical application.

## Acknowledgment

We would like to acknowledge the Intercollegiate Biomathematics Alliance for its funding to support this article.

## References


Adak, D. and N. Bairagi (2018). Analysis and computation of multi-pathways and multi-delays HIV-1 infection model. *Applied Mathematical Modelling 54*, 517–536. 134

Akiyama, H., C. M. Miller, C. R. Ettinger, A. C. Belkina, J. E. Snyder-Cappione, and S. Gummuluru (2018). HIV-1 intron-containing RNA expression induces innate immune activation and T-cell dysfunction. *Nature Communications 9*(1), 3450. 133

Andreu-Moreno, I., J.-V. Bou, and R. Sanjuán (2020). Cooperative nature of viral replication. *Science Advances 6*(49), eabd4942. 146

Archin, N. M., A. Espeseth, D. Parker, M. Cheema, D. Hazuda, and D. M. Margolis (2009). Expression of latent HIV induced by the potent HDAC inhibitor suberoylanilide hydroxamic acid. *AIDS Research and Human Retroviruses 25*(2), 207–212. 134

Chavali, A. K., V. C. Wong, and K. Miller-Jensen (2015). Distinct promoter activation mechanisms modulate noise-driven HIV gene expression. *Scientific Reports 5*, 17661. 134, 136, 138

Chou, S., H. Upton, K. Bao, U. Schulze-Gahmen, A. J. Samelson, N. He, A. Nowak, H. Lu, N. J. Krogan, Q. Zhou, et al. (2013). HIV-1 Tat recruits transcription elongation factors dispersed along a flexible AFF4 scaffold. *Proceedings of the National Academy of Sciences 110*(2), E123–E131. 134

Conway, J. M., A. S. Perelson, and J. Z. Li (2019). Predictions of time to HIV viral rebound following ART suspension that incorporate personal biomarkers. *PLoS Computational Biology 15*(7), e1007229. 134

Dave, R. S., P. Jain, and S. N. Byrareddy (2018). Follicular dendritic cells of lymph nodes as human immunodeficiency virus/simian immunodeficiency virus reservoirs and insights on cervical lymph node. *Frontiers in Immunology 9*. 133

Deeks, S. G., S. R. Lewin, and D. V. Havlir (2013). The end of AIDS: HIV infection as a chronic disease. *The Lancet 382*(9903), 1525–1533. 133

DeMarino, C., M. Cowen, M. L. Pleet, D. O. Pinto, P. Khatkar, J. Erickson, S. S. Docken, N. Russell, B. Reichmuth, T. Phan, et al. (2020). Differences in transcriptional dynamics between T-cells and macrophages as determined by a three-state mathematical model. *Scientific Reports 10*(1), 1–22. 134, 135, 136, 137, 140, 143, 145, 146

DeMarino, C., M. L. Pleet, M. Cowen, R. A. Barclay, Y. Akpamagbo, J. Erickson, N. Ndembe, M. Charurat, J. Jumare, S. Bwala, et al. (2018). Antiretroviral drugs alter the content of extracellular vesicles from HIV-1-infected cells. *Scientific Reports 8*(1), 7653. 133

Eaton, J. W., L. F. Johnson, J. A. Salomon, T. Bärnighausen, E. Bendavid, A. Bershteyn, D. E. Bloom, V. Cambiano, C. Fraser, J. A. Hontelez, et al. (2012). HIV treatment as prevention: systematic comparison of mathematical models of the potential impact of antiretroviral therapy on HIV incidence in south Africa. *PLoS Medicine 9*(7), e1001245. 134

Ferdin, J., K. Goričar, V. Dolžan, A. Plemenitaš, J. N. Martin, B. M. Peterlin, S. G. Deeks, and M. Lenassi (2018). Viral protein Nef is detected in plasma of half of HIV-infected adults with undetectable plasma HIV RNA. *PloS One 13*(1), e0191613. 133

Furtado, M. R., D. S. Callaway, J. P. Phair, K. J. Kunstman, J. L. Stanton, C. A. Macken, A. S. Perelson, and S. M. Wolinsky (1999). Persistence of HIV-1 transcription in peripheral-blood mononuclear cells in patients receiving potent antiretroviral therapy. *New England Journal of Medicine 340*(21), 1614–1622. 133

Garrido, C. and D. M. Margolis (2015). Translational challenges in targeting latent HIV infection and the CNS reservoir problem. *Journal of Neurovirology 21*(3), 222–226. 133

Gupta, V. and N. M. Dixit (2018). Trade-off between synergy and efficacy in combinations of HIV-1 latency-reversing agents. *PLoS Computational Biology 14*(2), e1006004. 134

Hatano, H., V. Jain, P. W. Hunt, T.-H. Lee, E. Sinclair, T. D. Do, R. Hoh, J. N. Martin, J. M. McCune, F. Hecht, et al. (2012). Cell-based measures of viral persistence are associated with immune activation and programmed cell death protein 1 (PD-1)–expressing CD4+ T-cells. *The Journal of Infectious Diseases 208*(1), 50–56. 133

Hatano, H., M. Somsouk, E. Sinclair, K. Harvill, L. Gilman, M. Cohen, R. Hoh, P. W. Hunt, J. N. Martin, J. K. Wong, et al. (2013). Comparison of HIV DNA and RNA in gut-associated lymphoid tissue of HIV-infected controllers and non-controllers. *AIDS (London, England) 27*(14), 2255. 133

Hayashi, T., M. Jean, H. Huang, S. Simpson, N. G. Santoso, and J. Zhu (2017). Screening of an FDA-approved compound library identifies levosimendan as a novel anti-HIV-1 agent that inhibits viral transcription. *Antiviral Research 146*, 76–85. 134

Heaton, R., D. Clifford, D. Franklin, S. Woods, C. Ake, F. Vaida, R. Ellis, S. Letendre, T. Marcotte, J. Atkinson, et al. (2010). HIV-associated neurocognitive disorders persist in the era of potent antiretroviral therapy: Charter study. *Neurology 75*(23), 2087–2096. 133, 145

Henderson, L. J., T. P. Johnson, B. R. Smith, L. B. Reoma, U. A. Santamaria, M. Bachani, C. Demarino, R. A. Barclay, J. Snow, N. Sacktor, et al. (2019). Presence of Tat and transactivation response element in spinal fluid despite antiretroviral therapy. *AIDS 33*, S145–S157. 133

Hill, A. L., D. I. Rosenbloom, F. Fu, M. A. Nowak, and R. F. Siliciano (2014). Predicting the outcomes of treatment to eradicate the latent reservoir for HIV-1. *Proceedings of the National Academy of Sciences 111*(37), 13475–13480. 134

Hladnik, A., J. Ferdin, K. Goričar, S. G. Deeks, B. M. Peterlin, A. Plemenitaš, V. Dolžan, and M. Lenassi (2017). Trans-activation response element RNA is detectable in the plasma of a subset of aviremic HIV-1–infected patients. *Acta Chimica Slovenica 64*(3), 530–536. 133

Hwang, T. J., D. Carpenter, J. C. Lauffenburger, B. Wang, J. M. Franklin, and A. S. Kesselheim (2016). Failure of investigational drugs in late-stage clinical development and publication of trial results. *JAMA Internal Medicine 176*(12), 1826–1833. 145

Jean, M. J., T. Hayashi, H. Huang, J. Brennan, S. Simpson, A. Purmal, K. Gurova, M. C. Keefer, J. J. Kobie, N. G. Santoso, et al. (2017). Curaxin cbl0100 blocks HIV-1 replication and reactivation through inhibition of viral transcriptional elongation. *Frontiers in Microbiology 8*, 2007. 134

Karn, J. (2000). Tat, a novel regulator of HIV transcription and latency. *HIV Sequence Compendium 1990*, 2–18. 146

Ke, R., J. M. Conway, D. M. Margolis, and A. S. Perelson (2018). Determinants of the efficacy of HIV latency-reversing agents and implications for drug and treatment design. *JCI Insight 3*(20). 134

Ke, R., S. R. Lewin, J. H. Elliott, and A. S. Perelson (2015). Modeling the effects of vorinostat in vivo reveals both transient and delayed HIV transcriptional activation and minimal killing of latently infected cells. *PLoS Pathogens 11*(10), e1005237. 134

Kessing, C. F., C. C. Nixon, C. Li, P. Tsai, H. Takata, G. Mousseau, P. T. Ho, J. B. Honeycutt, M. Fallahi, L. Trautmann, et al. (2017). In vivo suppression of HIV rebound by didehydro-cortistatin a, a block-and-lock strategy for HIV-1 treatment. *Cell Reports 21*(3), 600–611. 134

Khanna, I. (2012). Drug discovery in pharmaceutical industry: productivity challenges and trends. *Drug Discovery Today 17*(19-20), 1088–1102. 145

Kim, H., M.-S. Choi, K.-S. Inn, and B.-J. Kim (2016). Inhibition of HIV-1 reactivation by a telomerase-derived peptide in a hsp90-dependent manner. *Scientific Reports 6*, 28896. 134

Kim, J. B. and P. A. Sharp (2001). Positive transcription elongation factor B phosphorylates hSPT5 and RNA polymerase ii carboxyl-terminal domain independently of cyclin-dependent kinase-activating kinase. *Journal of Biological Chemistry 276*(15), 12317–12323. 146

Kumar, A., W. Abbas, and G. Herbein (2014). HIV-1 latency in monocytes/macrophages. *Viruses 6*(4), 1837–1860. 134

Kumar, A. M., I. Borodowsky, B. Fernandez, L. Gonzalez, and M. Kumar (2007). Human immunodeficiency virus type 1 RNA levels in different regions of human brain: quantification using real-time reverse transcriptase–polymerase chain reaction. *Journal of Neurovirology 13*(3), 210–224. 133

Lehrman, G., I. B. Hogue, S. Palmer, C. Jennings, C. A. Spina, A. Wiegand, A. L. Landay, R. W. Coombs, D. D. Richman, J. W. Mellors, et al. (2005). Depletion of latent HIV-1 infection in vivo: a proof-of-concept study. *The Lancet 366*(9485), 549–555. 134

Li, G.-H., L. Henderson, and A. Nath (2016). Astrocytes as an HIV reservoir: mechanism of HIV infection. *Current HIV Research 14*(5), 373–381. 133

Li, J., L. Peng, S. Gilmour, J. Gu, Y. Ruan, H. Zou, C. Hao, Y. Hao, and J. T.-f. Lau (2018). A mathematical model of biomedical interventions for HIV prevention among men who have sex with men in china. *BMC Infectious Diseases 18*(1), 600. 134

Li, J. Z., B. Etemad, H. Ahmed, E. Aga, R. J. Bosch, J. W. Mellors, D. R. Kuritzkes, M. M. Lederman, M. Para, and R. T. Gandhi (2016). The size of the expressed HIV reservoir predicts timing of viral rebound after treatment interruption. *AIDS (London, England) 30*(3), 343. 133

Lin, X., N. Kumari, C. DeMarino, Y. S. Kont, T. Ammosova, A. Kulkarni, M. Jerebtsova, G. Vazquez-Meves, A. Ivanov, K. Dmytro, et al. (2017). Inhibition of HIV-1 infection in humanized mice and metabolic stability of protein phosphatase-1-targeting small molecule 1e7-03. *Oncotarget 8*(44), 76749. 136

Mbonye, U. and J. Karn (2014). Transcriptional control of HIV latency: cellular signaling pathways, epigenetics, happenstance and the hope for a cure. *Virology 454*, 328–339. 134

McCauley, S. M., K. Kim, A. Nowosielska, A. Dauphin, L. Yurkovetskiy, W. E. Diehl, and J. Luban (2018). Intron-containing RNA from the HIV-1 provirus activates type I interferon and inflammatory cytokines. *Nature Communications 9*(1), 5305. 133

Mothobi, N. Z. and B. J. Brew (2012). Neurocognitive dysfunction in the highly active antiretroviral therapy era. *Current Opinion in Infectious Diseases 25*(1), 4–9. 133, 145

Mousseau, G., M. A. Clementz, W. N. Bakeman, N. Nagarsheth, M. Cameron, J. Shi, P. Baran, R. Fromentin, N. Chomont, and S. T. Valente (2012). An analog of the natural steroidal alkaloid cortistatin a potently suppresses Tat-dependent HIV transcription. *Cell Host & Microbe 12*(1), 97–108. 134

Mousseau, G., C. F. Kessing, R. Fromentin, L. Trautmann, N. Chomont, and S. T. Valente (2015). The Tat inhibitor didehydrocortistatin a prevents HIV-1 reactivation from latency. *MBio 6*(4), e00465–15. 134

Narayanan, A., S. Iordanskiy, R. Das, R. Van Duyne, S. Santos, E. Jaworski, I. Guendel, G. Sampey, E. Dalby, M. Iglesias-Ussel, et al. (2013). Exosomes derived from HIV-1-infected cells contain trans-activation response element RNA. *Journal of Biological Chemistry 288*(27), 20014–20033. 133

Omondi, E., R. Mbogo, and L. Luboobi (2018). Mathematical analysis of sex-structured population model of HIV infection in Kenya. *Letters in Biomathematics 5*(1), 174–194. 134

Perelson, A. S. and P. W. Nelson (1999). Mathematical analysis of HIV-1 dynamics in vivo. *SIAM Review 41*(1), 3–44. 134

Rutsaert, S., J.-M. Steens, P. Gineste, B. Cole, S. Kint, P. N. Barrett, J. Tazi, D. Scherrer, H. J. Ehrlich, and L. Vandekerckhove (2019). Safety, tolerability and impact on viral reservoirs of the addition to antiretroviral therapy of ABX464, an investigational antiviral drug, in individuals living with HIV-1: a phase IIa randomised controlled study. *Journal of Virus Eradication 5*(1), 10. 134

Sampey, G. C., M. Saifuddin, A. Schwab, R. Barclay, S. Punya, M.-C. Chung, R. M. Hakami, M. A. Zadeh, B. Lepene, Z. A. Klase, et al. (2016). Exosomes from HIV-1-infected cells stimulate production of pro-inflammatory cytokines through trans-activating response (TAR) RNA. *Journal of Biological Chemistry 291*(3), 1251–1266. 133

Sengupta, S. and R. F. Siliciano (2018). Targeting the latent reservoir for HIV-1. *Immunity 48*(5), 872–895. 133

UNAIDSDate (2019, Jan). Global statistics. 133

Van Duyne, R., I. Guendel, E. Jaworski, G. Sampey, Z. Klase, H. Chen, C. Zeng, D. Kovalskyy, M. H. El Kouni, B. Lepene, et al. (2013). Effect of mimetic CDK9 inhibitors on HIV-1-activated transcription. *Journal of Molecular Biology 425*(4), 812–829. 136

Velasco-Hernandez, J. X., H. Gershengorn, and S. M. Blower (2002). Could widespread use of combination antiretroviral therapy eradicate HIV epidemics? *The Lancet Infectious Diseases 2*(8), 487–493. 134

Wang, X., X. Song, S. Tang, and L. Rong (2016). Dynamics of an HIV model with multiple infection stages and treatment with different drug classes. *Bulletin of Mathematical Biology 78*(2), 322–349. 134

Wei, D. G., V. Chiang, E. Fyne, M. Balakrishnan, T. Barnes, M. Graupe, J. Hesselgesser, A. Irrinki, J. P. Murry, G. Stepan, et al. (2014). Histone deacetylase inhibitor romidepsin induces HIV expression in CD4 T-cells from patients on suppressive antiretroviral therapy at concentrations achieved by clinical dosing. *PLoS Pathogens 10*(4), e1004071. 134

Weinberger, L. S., J. C. Burnett, J. E. Toettcher, A. P. Arkin, and D. V. Schaffer (2005). Stochastic gene expression in a lentiviral positive-feedback loop: HIV-1 Tat fluctuations drive phenotypic diversity. *Cell 122*(2), 169–182. 145, 146

Weinberger, L. S. and T. Shenk (2006). An HIV feedback resistor: auto-regulatory circuit deactivator and noise buffer. *PLoS Biology 5*(1), e9. 145

Wodarz, D. and M. A. Nowak (2002). Mathematical models of HIV pathogenesis and treatment. *BioEssays 24*(12), 1178–1187. 134